

Theoretical Investigation of Pd-catalyzed Carbo-aminative Annulation of 1,6-enyne with 2-Iodoaniline Via 6-Endo-Trig Mode

Nan Lu*, Chengxia Miao and Xiaozheng Lan

College of Chemistry and Material Science, Shandong Agricultural University, Taian City, P.R. China

*Corresponding Author: Nan Lu, College of Chemistry and Material Science, Shandong Agricultural University, Taian City, P.R. China.

Received: March 13, 2023

Published: May 24, 2023

© All rights are reserved by Nan Lu, *et al.*

DOI:10.31080/ASPS.2023.07.0960

Abstract

The mechanism is investigated for Pd-catalyzed carbo-aminative cyclization of 1,6-enyne with 2-iodoaniline. The regioselective addition of Pd-inserted 2-iodoaniline across alkyne and intermolecular insertion of olefin leads to alkyne-to-alkene adducts. After olefin isomerization, a pallado intermediate is obtained upon aza-conjugate addition. The β -hydride is eliminated with the help of Pd. The oxidative aromatization promoted by carbonate ion makes the oxidation level consistent with desired product. The regioselectivity of 6-endo-trig cyclization is determined through the superiority over other two modes in Heck-type intramolecular coupling. The promotion of active Pd(0) lies in the barrier decrease of rate-limiting olefin isomerization and aza-conjugate addition especially the β -hydride elimination. These results are supported by Multiwfn analysis on FMO of specific TSs and MBO value of vital bonding, breaking.

Keywords: Annulation; 1,6-enynes; Regioselectivity; 6-endo-trig; Aryl Palladation

Introduction

As an attractive field, the emergence of 1,6-enynes within organic chemistry has greatly accelerated the development of synthetic diversifications and allowed us to realize molecular complexity through valuable cascade transformations [1]. A variety of elusive cyclic systems have been stimulated to explore their substitution extent and reactive pattern. Enormous progress has been achieved in the production of five-membered (hetero) cycles using 1,6-enynes in transition-metal-catalyzed cycloisomerizations [2,3] and reductive cyclization [4]. Among advances of this line, there is lots of interesting transition-metal-catalyzed hydrofunctionalization cyclization, such as alkyne-to-alkene cyclization via 5-exo-trig manner and alkene-to-alkyne 5-exo-dig pathways initiated by radical generated at the olefin end [5-8]. Recently, the iodide-catalyzed

radical reductive cyclization with various vinyl halides and cobalt-catalyzed intermolecular hydroarylation/cyclization of 1,6-enynes with N-pyridylindoles have gained much attention [9,10]. In contrast, three types of novel metal-catalyst-free radical cyclization with sulfonyl hydrazides have realized selective and switchable synthesis of lactams in water [11]. The seleno-dibenzocycloheptenones and seleno-spiro[5.5]-trienones can be synthesized through radical cyclization of biaryl ynones in the presence of diorganyl diselenides [12].

As indispensable constituents in pharmaceutical and agrochemical industry, naphthyridinones are vital fragments owing to their broad range of biological activities [13]. Although fused nitrogen heterocycles are extensively found in nature, the efficient and rapid construction has been facing challenge for synthetic chemists [14].

As molecules of great interest, a wide variety of naphthyridinones have gained attention by increasing demand of new drug discoveries [15,16]. To assemble N-heterocycles in selective and proficient way, cascade reactions are most often used for the concise construction of diverse heterocyclic architectures [17]. Besides enzymatic version in biosynthesis [18], the radical cascade cyclization can be used to construct bicyclic structures with controlling enantioselectivity and diastereoselectivity [19]. Recently, the palladium-catalyzed method has become the focus of attention. Reisman has summarized its strategic applications involving C–C and C–X bond formation in natural product synthesis [20]. Saracoglu has realized directed C–H functionalization of free (NH) indoles with iodoarenes substituted by aldehyde, ketone, and acid/ester via palladium catalysis [21]. Patel has also reported Pd(II)-catalyzed synthesis of furo[2,3-b]pyridines from β -ketodinitriles and alkynes via cyclization and N–H/C annulation [22].

Based on the reactivity of activated alkynes, a series of novel N-heterocycles were synthesized through concise and pragmatic methods, such as Reddy's regioselective cascade annulation for fused polyheterocycles in harnessing Rh-catalyzed C–H activation [23] and annulation of phenacyl ammonium salts with propargylic alcohols also catalyzed by Rh via sequential dual C–H and C–C activation to diverse isochromenones [24]. In a recent experiment, Reddy has developed another carbo-aminative cyclization of 1,6-enynes catalyzed by Pd toward naphthyridinone derivatives [25]. This represents a rare endo-trig mode toward 1,1-difunctionalization of olefin different from previous exo-trig/endo-dig mode through 1,2-difunctionalization [26]. However, there is no answer to why the current method gave 6-endo-trig products and lack of comparison with possible reaction paths majorly determining the selectivity of cyclization. Are there any other orientations of the first insertion of aryl-palladium complex to alkyne moiety just like two insertion paths of hydride-palladium species to alkyne reported by Petrone [27]? To solve these problems in experiment, we carried out theoretical research thoroughly in description of detailed mechanism for this effective method especially the regioselective aryl palladation of alkyne and the following Heck-type intramolecular coupling. The goal of our study is to clarify the real process of this novel annulative cyclization affording polycyclic motifs.

Methods

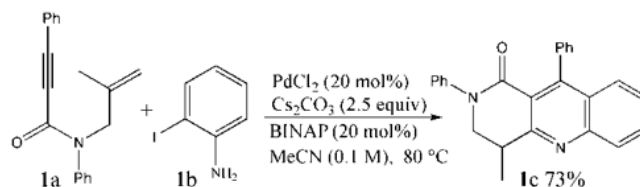
The geometry optimizations were performed at the B3LYP/BSI level with the Gaussian 09 package [28,29]. The mixed basis set of LanL2DZ for Pd, I and 6-31G(d) for nonmetal atoms [30–34] was denoted as BSI. Different singlet and multiplet states were clarified with B3LYP and ROB3LYP approaches including Becke's three-parameter hybrid functional combined with Lee–Yang–Parr correction for correlation [35,36]. The nature of each structure was verified by performing harmonic vibrational frequency calculations. Intrinsic reaction coordinate (IRC) calculations were examined to confirm the right connections among key transition-states and corresponding reactants and products. Harmonic frequency calculations were carried out at the B3LYP/BSI level to gain zero-point vibrational energy (ZPVE) and thermodynamic corrections at 353.15 K and 1 atm for each structure in acetonitrile (MeCN). The solvation-corrected free energies were obtained at the B3LYP/6-311++G(d,p) (LanL2DZ for Pd, I) level in MeCN by using integral equation formalism polarizable continuum model (IEFPCM) in Truhlar's "density" solvation model [37–41] on the B3LYP/BSI-optimized geometries.

As an efficient method obtaining bond and lone pair of a molecule from modern ab initio wave functions, NBO procedure was performed with Natural bond orbital (NBO3.1) to characterize electronic properties and bonding orbital interactions [42–44]. The wave function analysis was provided using Multiwfn_3.7_dev package [45] including composition of frontier molecular orbital (FMO) and Mayer bond order (MBO).

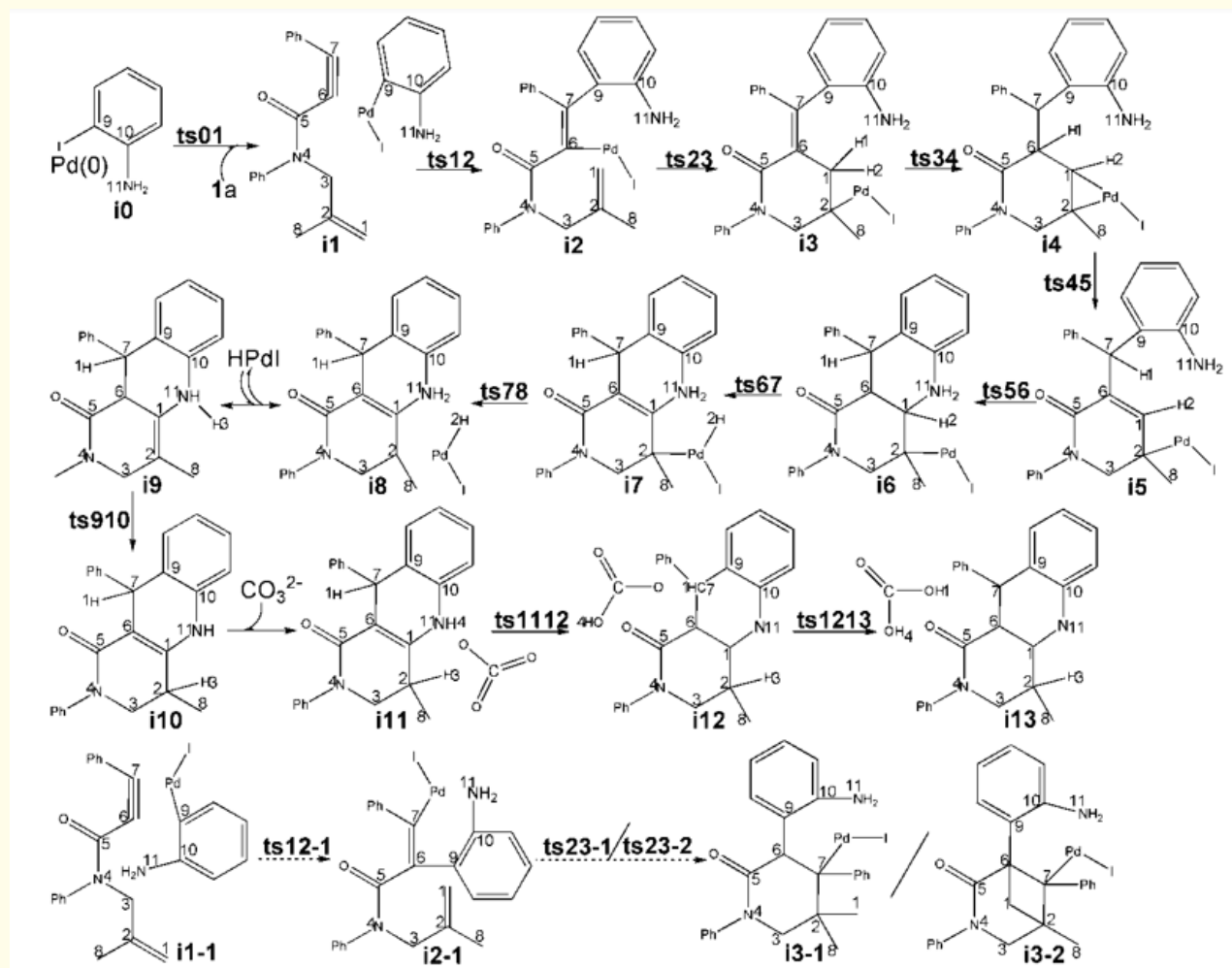
Results and Discussion

The mechanism was projected for the carbo-aminative cyclization of nitrogen-tethered 1,6-enyne 1a with 2-iodoaniline 1b toward naphthyridinone derivative 1c catalyzed by Pd (Scheme 1). In view of the fact that what really plays a catalytic role is the in-situ-generated active Pd(0) [25], Pd(0) was only considered in our mechanism research. As illustrated by Scheme 2, the process includes: (1) oxidative addition of Pd(0) to 1b giving aryl-palladium complex, the regioselective insertion of which to 1a giving i2 followed by another intermolecular insertion from alkene to Pd–C bond leading to i3, (2) olefin isomerization through two steps affording i5, which is converted to i6 upon aza-conjugate addition,

(3) the elimination of β -hydride and departure of HPdI via two steps resulting in *i*9, which upon isomerization furnishes *i*10, (4) the oxidative aromatization with the help of carbonate ion affording desired product *1c*. Figure 1 and Supplementary Figure S1 list the optimized structures of TSs and intermediates in Scheme 2, respectively. Table 1 and Supplementary Table S1 show the activation energy of all reactions and the relative energies of all stationary points. Since the reaction occurred in MeCN in experiment, the Gibbs free energies in solution phase are mainly discussed here.



Scheme 1: Pd-catalyzed carbo-aminative cyclization of nitrogen-tethered 1,6-enyne *1a* with 2-iodoaniline *1b* toward naphthyridinone derivative *1c*.



Scheme 2: Proposed reaction pathway of Pd-catalyzed carbo-aminative cyclization of nitrogen-tethered 1,6-enyne *1a* with 2-iodoaniline *1b*. The initial complex between *1a* and Pd(0)-inserted *1b* is denoted as *i*1. TS is named according to the two intermediates it connects.




Figure 1: Optimized structure of transition states for Pd-catalyzed annulation of 1a with 1b (Bond lengths in angstroms).

TS	ΔG^*_{gas}	ΔG^*_{sol}
ts01	2.8	3.1
ts12	15.5	17.0
ts23	10.2	12.8
ts12-1	10.2	10.6
ts23-1	50.9	55.4
ts23-2	66.4	67.9
ts34	37.4	37.7
ts45	21.0	17.9
ts56	29.0	26.4
ts67	-1.5	-2.1
ts78	20.9	22.3
ts910	22.2	32.6
ts1112	0.6	1.3
ts1213	6.7	11.2

Table 1: The activation energy (in kJ mol^{-1}) of all reactions in gas and solvent.

Regioselective aryl palladation of alkyne and intermolecular insertion from alkene to Pd-C bond

The oxidative addition of Pd(0) to 1b takes place via ts01 with a low activation energy barrier of 3.1 kJ mol^{-1} . After binding al-

kyne 1a, an initial complex i1 is generated involving Pd(II) with a relative energy 9.3 kJ mol^{-1} lower than isolated species. As the starting point of relative Gibbs free energy profile (path A of Figure 2), the energy of i1 is set as 0.0 kJ mol^{-1} , from which the regioselective insertion to alkyne occurs in step 1 via ts12 to achieve the concerted addition of aryl-to-alkyne and alkyne-to-Pd with an activation energy of 17.0 kJ mol^{-1} leading to i2. The transition vector corresponds to remarkable breaking of C9-Pd bond (2.06 \AA), linking of C9-C7 (2.04 \AA), C6-Pd (2.05 \AA) and elongation of C6-C7 triple bond to double (1.28 \AA) (Supplementary Figure S2a). To get more qualitative evidence of structural analysis, the visual orbitals of Highest Occupied Molecular Orbital (HOMO) and Lowest Unoccupied Molecular Orbital (LUMO) are analyzed applying FMO calculations of typical transition states (Figure 3) together with MBO analysis for the orbital contribution of bonding atoms (Table 2 and Table 3) [30-34]. HOMO of ts12 on C9, C6 (5.29%, 4.30%) and LUMO on C7, Pd (3.07%, 29.17%) is ready for the concerted aryl-to-alkyne and alkyne-to-Pd attack. MBO values of C6...Pd, C9...Pd (0.659, 0.729) verify the forming and breaking of C6-Pd, C9-Pd bond. The resultant i2 is rather stable with the exergonic energy high to be $-30.8 \text{ kJ mol}^{-1}$.

Figure 2: Relative Gibbs free energy profile in solvent phase starting from complex i1 and i1-1.

Figure 3: Highest Occupied Molecular Orbital (HOMO) and Lowest Unoccupied Molecular Orbital (LUMO) of typical transition states ts12, ts23, ts23-1, ts23-2, and ts56. Different colors are used to identify the phase of the wave functions.

	C6	C7	C9	Pd	
ts12 HOMO	4.30	1.74	5.29	11.56	
ts12 LUMO	21.65	3.07	11.32	29.17	
	C1	C2	C6	Pd	
ts23 HOMO	0.52	0.13	1.87	9.31	
ts23 LUMO	11.71	1.15	15.36	9.65	
	C1	C2	C6	C7	Pd
ts23-1 HOMO	16.20	2.94	26.64	4.10	6.96
ts23-1 LUMO	44.79	0.82	13.78	6.16	1.26
	C1	C2	C6	C7	Pd
ts23-2 HOMO	1.97	29.67	1.01	28.59	4.01
ts23-2 LUMO	1.46	37.85	1.15	20.33	3.10
	C1	C6	N11	Pd	
ts56 HOMO	4.98	46.36	9.00		
ts56 LUMO	0.56	1.95	0.57	39.52	

Table 2: Contribution (%) of Natural Atomic Orbital (NAO) to Highest Occupied Molecular Orbital (HOMO), and Lowest Unoccupied Molecular Orbital (LUMO) of typical TSs.

	C7...C9	C6...Pd	C9...Pd	C6...C7	
ts12	0.422	0.659	0.729	1.751	
	C1...C6	C2...Pd	C6...Pd	C1...C2	
ts23	0.431	0.679	0.626	1.100	
	C2...C7	C1...C2	C6...C7	C7...Pd	
ts23-1	0.672	1.243	1.127	0.769	
	C1...C6	C2...C7	C1...C2	C6...C7	C7...Pd
ts23-2	0.828	0.320	1.185	1.040	0.920
	N11...C1	C1...C6	C10...N11		
ts56	0.481	1.261	0.816		

Table 3: Mayer bond order (MBO) of typical TSs.

Step 2 is the intermolecular insertion from alkene to Pd-C bond via ts23 affording stable i3 continuously releasing heat by 35.9 kJ mol⁻¹. The activation energy barrier is 12.8 kJ mol⁻¹ together with the energy level of ts23 even lower than zero (-18.0 kJ mol⁻¹), this step is supposed to be fairly easy. The transition vector indicates the electrophilic attack of alkyne-to-alkene with the coordination of Pd changing from alkyne C6 to alkene C2 simultaneously. Thus this cyclization is verified to be 6-endo-trig mode involving bonding of C1-C6, departure of Pd from C6 to C2 (2.05, 2.08, 2.11 Å), and the elongation of C1-C2 double bond to single (1.44 Å) (Figure S2b). In resultant i3, the new six-membered ring and Pd-C2 coordinated bond (2.03 Å) represent the completion of regioselective aryl palladation of alkyne and intermolecular insertion of olefin.

The selectivity of 6-endo-trig product is supposed to be majorly determined by the orientation of the first insertion of aryl-palladium complex to alkyne. Inspired by two insertion paths of hydride-palladium species to alkyne [27], an alternative alkyne insertion (path B and C of Figure 2) was explored by modeling a rotation of Pd-I fragment parallel to C≡C bond. As is described by the dashed arrow of Scheme 2, step 1 takes place via ts12-1 with activation energy of 10.6 kJ mol⁻¹ relative to the initial complex i1-1 of path B. The transition vector concerns the breaking of C9-Pd and forming of C6-C9, C7-Pd (2.06, 2.14, 2.07 Å) bond. As their counterparts, the energy level of both ts12-1 and i2-1 are also similar with ts12 and i2 of path A. Therefore, path B is no better than path A kinetically and thermodynamically for aryl palladation of alkyne. From i2-1, two possible cyclization modes exist based on the Mulliken charge of atoms C1 (-0.40), C2 (0.23), C6 (-0.02) and C7 (-0.15). On one hand, the nucleophilic attack of negative C7 (-0.15) to positive C2 (0.23) via ts23-1 is determined to be alkyne-to-alkene 6-exo-trig cyclization in step 2. The transition vector corresponds to prominent approaching of C7 to C2 (1.81 Å), and the cooperative stretching of C1-C2, C6-C7 (1.42, 1.45 Å) (Figure S2c). There is no change for the coordinated C7-Pd and N11-Pd bonds (2.11, 2.15 Å) in this process of path B. Given the activation energy high to be 55.4 kJ mol⁻¹ and the endothermic energy of 6.2 kJ mol⁻¹ resulting in i3-1, path B is disfavored both from kinetics and thermodynamics.

On the other, like ts23 of path A, alkyne C6 (-0.02) also could attack alkene C1 (-0.40) via ts23-2 forming i3-2 in step 2, which is located as path C. Seen from the transition vector (Figure S2d), besides the evident bonding of C1-C6 (1.65 Å), the C2...C7 distance is shortening synchronously. Thereby a four membered ring assembled by C1-C6, C2-C7, C1-C2 and C6-C7 single bonds (1.56, 1.57, 1.54, 1.57 Å) stands above the six membered ring in resultant i3-2, making this cyclization not a simple 6-endo-trig mode. Similar with path B, there is no coordination transfer in path C with C7 and N11 still bonding to Pd (1.99, 2.16 Å). Despite the bicyclic structure of i3-2 makes it much more stable than i3-1, the activation energy of path C is even higher by 12.5 kJ mol⁻¹ than that of path B. Once via path B or C, two barriers are both too high. The reaction should be stopped at this step. FMO results also support the superiority of ts23 over other two modes of ts23-1 and ts23-2. For ts23, HOMO and LUMO is main on Pd, C6 (9.31%, 1.87%) on C6, C1 (15.36%, 11.71%) allowing for the alkyne-to-alkene addition and coordina-

tion shift of Pd giving 6-endo-trig product. The accompanied bonding can be demonstrated by MBO values of C1...C6, C2...Pd (0.431, 0.679). Nevertheless, for ts23-1, HOMO and LUMO is only minor on the attacking C7 and attacked C2 (4.10%, 0.82%) to realize 6-exo-trig mode. The unfavorable conditions also exist in the contribution of C6 on HOMO and C1 on LUMO (1.01%, 1.46%) of ts23-2. Hence, path A is selected as the most favored energetically through comparison with alternative possible alkyne insertion. This not only rationalizes the regioselectivity of aryl palladation in step 1 but confirms the 6-endo-trig cyclization mode of step 2.

Olefin isomerization, aza-conjugate addition and β-hydride elimination

Initiated from i3, the next olefin isomerization proceeds via the following step 3 and step 4 which are essentially two times of proton transfer. Illustrated by the relative Gibbs free energy profile (Figure 2), the proton H1 shifts from C1 to C6 (1.35, 1.25 Å) via ts34 with an activation energy barrier of 37.7 kJ mol⁻¹ with respect to i3 (Figure S2e). From the energy level of i4 (-25.7 kJ mol⁻¹), it is more reactive than i3 owing to the transient ternary ring with tension formed between Pd and C1-C2 bond. The second proton transfer from C6 to C7 (1.27, 1.51 Å) takes place via ts45 exergonic by -42.3 kJ mol⁻¹ (Figure S2f). The activation energy of step 4 is decreased to be 17.9 kJ mol⁻¹ owing to the negative energy level of ts45 (-7.8 kJ mol⁻¹). Once H1 is bonded to C7, the standard sp³ hybridization at C7, normal C1-C6 double bond and vanishing ternary ring shapes a rather stable intermediate i5 causing step 4 quite readily accessible. The aza-conjugate addition proceeds in step 5 via ts56, the transition vector of which includes the approaching of N11...C1 (1.81 Å) and the cooperating elongation of C1-C6, C10-N11 bond (1.41, 1.46 Å) (Figure S2g). The activation energy barrier is 26.4 kJ mol⁻¹ exergonic by -34.7 kJ mol⁻¹ forming pallado intermediate i6, in which the closure of a new six membered azacycle is completed with C1-N11 and C1-C6 single bond (1.52, 1.49 Å). For ts56 representing the second typical cyclization, the electron density of HOMO main on N11 (9.00%) minor on C1, C6 (0.56%, 1.95%) favors aza-conjugate addition. MBO value of N11...C1 (0.481) suggests the ongoing heterocyclization.

The β-hydride elimination of step 6 occurs via ts67 yielding i7, which is converted to i8 in step 7 via ts78 upon the breaking of

C2-Pd (2.29 Å) and departure of HPdI fragment. Both of these two steps are fairly easy with quiet low energy level of ts67 and ts78 (-36.8 and -31.0 kJ mol⁻¹). The transition vector of ts67 is about the transfer of proton H2 from C1 to Pd (1.41, 1.76 Å) and the contraction of C1-C6 single bond to double (1.39 Å) (Figure S2h). Till the cleavage of HPdI, with the participation of active Pd(0), step 3 is determined to be rate-limiting from the activation energy perspective for the whole process of carbo-aminative cyclization between 1a and 1b. Despite the barrier of ts34 (37.7 kJ mol⁻¹) is somewhat high, the rate constant *k* is calculated to be about 3.3*10⁻¹¹ s⁻¹ applying the experimental temperature (80 °C). Thereby, the value with B3LYP/6-311++G(d,p) (LanL2DZ for Pd, I) method indicates that the barrier of proton transfer is completely possible to overcome. Moreover, the exergonic energy -47.0 kJ mol⁻¹ of the final intermediate i8 suggests this reaction favorable from thermodynamics.

Isomerization and oxidative aromatization

Without HPdI, an intermediate i9 is located as a new starting point of isomerization. As shown by the black dash line of Figure 4, this last olefin isomerization is accomplished via ts910 with a relatively high barrier of 32.5 kJ mol⁻¹ without the participation of Pd catalyst. The transition vector of ts910 is also a proton transfer mode N11...H3...C2 (1.25, 1.73 Å). When the double bond between C1, C2 moves to between C1, N11, and the final complex i10 is yielded lower by 52.0 kJ mol⁻¹ in energy level than that of i9 approved to be advantageous. Considering the oxidation level of i10 is not consistent with the desired product 1c, the calculation model of oxidative aromatization with the help of carbonate ion CO₃²⁻ is established and depicted by the red dash line of Figure 4. The initial complex i11 binds CO₃²⁻ and i10 with N11-H4...O hydrogen bond (1.90 Å). As step 1, the first dehydrogenation oxidation takes place via ts1112 with a small activation energy barrier of 1.3 kJ mol⁻¹ relative to the starting point i11 exergonic by -8.5 kJ mol⁻¹. The transition vector indicates the migration of H4 from N11 to CO₃²⁻ (1.32, 1.19 Å) forming hydrogen carbonate HCO₃⁻ in the resultant i12, where the hydrogen bond turns to be O-H4...N11 (2.37 Å). Via ts1213, the second dehydrogenation oxidation proceeds in step 2 forming i13 also exergonic by -9.9 kJ mol⁻¹. The activation energy is uphill to be 11.2 kJ mol⁻¹ still low to overcome. The transition vector concerns the departure of another H1 by HCO₃⁻ from C7 (1.36 1.29 Å). Gaining two hydrogen atoms, HCO₃⁻ becomes carbonic acid H₂CO₃ in the last i13 with two strong hydrogen bonds O-H...O

(1.67, 1.68 Å). Step 2 is determined to be rate-limiting for oxidative aromatization promoted by CO₃²⁻ kinetically and thermodynamically favored.

Figure 4: Relative Gibbs free energy profile in solvent phase starting from complex i9 and i11.

Solvent effect

Without ions, the solvent effect is expected to be small on this neutral system [30-34]. The difference of relative energy and activation energy barrier between in gas phase and MeCN solution are listed for all stationary points (Table S1 and Table S2). The absolute energies in solution phase are decreased by -20~-30 kJ mol⁻¹ from those in gas phase for all optimized structures. The reduced degree of TSs is larger than that of intermediates. There is little difference between relative energies in solution and those in gas phase for regioselective insertion to alkyne and intermolecular insertion of olefin in step 1 and 2. In the following five steps of olefin isomerization, aza-conjugate addition and β-hydride elimination catalyzed by Pd(0), the reduction extent of relative energies is relatively large (-2~-11 kJ mol⁻¹). The case is similar for oxidative aromatization promoted by CO₃²⁻ with decreased degree less than -12.0 kJ mol⁻¹. Generally, the normal influence of solvent from kinetics is to reduce the energy barrier in gas phase. The larger the reduction value, the more readily the path. From this point, the last five steps are advantageous over the first two steps with decreased energy level of TSs. The β-hydride elimination via ts67 in step 6 is the most affected with a downhill of -11.0 kJ mol⁻¹. In addition, the impact on olefin

isomerization and aza-conjugate addition are also obvious with reduced values of -1.8, -4.6, and -4.1 kJ mol⁻¹ for ts34, ts45, and ts56, respectively. Accordingly, the influence of solvation on Pd-catalyzed carbo-aminative cyclization of nitrogen-tethered 1,6-enyne with 2-iodoaniline is advantageous from a kinetic point of view.

Conclusion

Our DFT calculations provide the first theoretical investigation on carbo-aminative cyclization of 1,6-enynes with 2-iodoaniline catalyzed by Pd. The addition of Pd-inserted 2-iodoaniline across alkyne occurs regioselectively and then the intermolecular insertion of olefin leads to alkyne-to-alkene adducts. After the following olefin isomerization, a pallado intermediate is obtained upon aza-conjugate addition. The β -hydride is eliminated and HPdI is departed with the help of Pd. The second isomerization produces a more stable bicyclo structure, the oxidative aromatization of which promoted by carbonate ion makes the oxidation level consistent with the desired product.

Compared with those in gas phase, the decreased relative energies of stationary points and activation energy barriers in solution denote an advantageous solvation effect kinetically. Two possible insertion paths exist in aryl palladation of alkyne. The regioselectivity of 6-endo-trig cyclization is determined through the superiority over other two modes in Heck-type intramolecular coupling. The promotion of active Pd(0) lies in the barrier decrease of rate-limiting olefin isomerization and aza-conjugate addition especially the β -hydride elimination. These results are supported by Multiwfn analysis on FMO of specific TSs and MBO value of vital bonding, breaking.

Acknowledgements

This work was supported by National Natural Science Foundation of China (21973056, 21972079) and Natural Science Foundation of Shandong Province (ZR2019MB050).

Bibliography

1. Marinetti A., *et al.* "Enantioselective, transition metal catalyzed cycloisomerizations". *Chemical Society Reviews* 41.14 (2012): 4884-4908.
2. Deng X., *et al.* "Enantioselective Rhodium-Catalyzed Cycloisomerization of 1,6-Allenynes to access 5/6-Fused Bicycle[4.3.0]-nonadienes". *Nature Communication* 10.1 (2019): 949 (1-10).
3. Liang RX., *et al.* "Palladium-Catalyzed Enantioselective Heteroarenyne Cycloisomerization Reaction". *Angewandte Chemie Int. Ed.* 60.13 (2021): 7412-7417.
4. Park JH., *et al.* "Rh-Catalyzed Reductive Cyclization of Enynes using Ethanol as a Source of Hydrogen". *Chemistry: A European Journal* 17.39 (2011): 10852-10856.
5. Ren X., *et al.* "Enantioselective Hydroesterificative Cyclization of 1,6-Enynes to Chiral γ -Lactams Bearing a Quaternary Carbon Stereocenter". *Organic Letters* 23.9 (2021): 3561-3566.
6. Dong M., *et al.* "PhI (OAc)₂-Mediated Dihalogenative Cyclization of 1,6-Enyne with Lithium Halide". *Organic Letters* 23.9 (2021): 3588-3592.
7. Whyte A., *et al.* *Journal of the American Chemical Society* 142.20 (2020): 9510-9517.
8. Xuan J., *et al.* *Organic Letters* 18.24 (2016): 6372-6375.
9. Ding L., *et al.* "Merging Hydrogen Atom Transfer and Halogen Atom Transfer for Iodide-Catalyzed Radical Reductive Cyclization of 1,6-Enynes". *Organic Letters* 24.17 (2022): 3113-3117.
10. Yu XC., *et al.* "Metal-Catalyst-Free Radical Cyclization of 1,6-Enynes for the Selective and Switchable Synthesis of Lactams in Water". *ACS Sustainable Chemistry and Engineering* 10.18 (2022): 6057-6062.
11. Kong D., *et al.* "Mechanism and Origins of Enantioselectivity of Cobalt-Catalyzed Intermolecular Hydroarylation/Cyclization of 1,6-Enynes with *N*-Pyridylindoles". *The Journal of Organic Chemistry* 87.9 (2022): 6438-6443.
12. Goulart HA., *et al.* "Synthesis of Seleno-Dibenzocycloheptenones/Spiro[5.5]Trienones by Radical Cyclization of Biaryl Ynones". *The Journal of Organic Chemistry* 87.6 (2022): 4273-4283.
13. Zhuo LS., *et al.* "Structure reactivity relationship study of novel quinazoline-based 1,6-naphthyr-idinones as MET inhibitors with potent antitumor efficacy". *European Journal of Medicinal Chemistry* 208 (2020): 112785-112801.
14. Heravi MM., *et al.* "Prescribed drugs containing nitrogen heterocycles: an overview". *RSC Advances* 10.72 (2020): 44247-44311.

15. Saldívar-González FI, *et al.* "Exploring the Chemical Space and the Bioactivity Profile of Lactams: a Chemo-informatic Study. Exploring the chemical space and the bioactivity profile of lactams: a chemoinformatic study". *RSC Advances* 9.46 (2019): 27105-27116.
16. Wang MS, *et al.* "Efficient Arylation of 2,7-Naphthyridin-1 (2H)-one with Diaryliodonium Salts and Discovery of a New Selective MET/AXL Kinase Inhibitor". *ACS Combinatorial Science* 22.9 (2020): 457-467.
17. Lu LQ, *et al.* "Development of Cascade Reactions for the Concise Construction of Diverse Heterocyclic Architectures". *Accounts of Chemical Research* 45.8 (2012): 1278-1293.
18. Walsh T, *et al.* "Enzymatic Cascade Reactions in Biosynthesis". *Angewandte Chemie Int. Ed.* 58.21 (2019): 6846-6879.
19. Zhang C, *et al.* "Controlling Enantioselectivity and Diastereoselectivity in Radical Cascade Cyclization for Construction of Bicyclic Structures". *Journal of the American Chemical Society* 143.29 (2021): 11130-11140.
20. Holman KR, *et al.* "Palladium-catalyzed cascade cyclizations involving C-C and C-X bond formation: strategic applications in natural product synthesis". *Chemical Society Reviews* 50.14 (2021): 7891-7908.
21. Taskesenligil Y, *et al.* "Directed C-H Functionalization of C3-Aldehyde, Ketone, and Acid/Ester-Substituted Free (NH) Indoles with Iodoarenes via a Palladium Catalyst System". *The Journal of Organic Chemistry* 88.3 (2023): 1299-1318.
22. Rakshit A, *et al.* "Pd (II)-Catalyzed Synthesis of Furo[2,3-b]pyridines from β -Ketodinitriles and Alkynes via Cyclization and N-H/C Annulation". *Organic Letters* 24.20 (2022): 3741-3746.
23. Singam MKR, *et al.* "Harnessing Rhodium-Catalyzed C-H Activation: Regioselective Cascade Annulation for Fused Polyheterocycles". *The Journal of Organic Chemistry* 86.12 (2021): 8069-8077.
24. Singam MKR, *et al.* "Rhodium-Catalyzed Annulation of Phenacyl Ammonium Salts with Propargylic Alcohols via a Sequential Dual C-H and a C-C Bond Activation: Modular Entry to Diverse Isochromenones". *Organic Letters* 23.20 (2021): 7888-7893.
25. Babu US, *et al.* "Palladium-Catalyzed Carbo-Aminative Cyclization of 1,6-Enynes: Access to Naphthyridinone Derivatives". *Organic Letters* 24.8 (2022): 1598-1603.
26. Zhu S, *et al.* "Three-Component Radical Iodonitrosylative Cyclization of 1,6-Enynes under Metal-Free Conditions". *Organic Letters* 23.13 (2021): 5044-5048.
27. Petrone DA, *et al.* "Palladium-Catalyzed Hydrohalogenation of 1,6-Enynes: Hydrogen Halide Salts and Alkyl Halides as Convenient HX Surrogates". *Journal of the American Chemical Society* 139.9 (2017): 3546-3557.
28. Frisch, MJ, *et al.* Gaussian 09, Revision B.01, Gaussian, Inc, Wallingford, CT (2009).
29. Hay PJ, *et al.* "Ab initio effective core potentials for molecular calculations-potentials for the transition-metal atoms Sc to Hg". *The Journal of Chemical Physics* 82.1 (1985): 270-283.
30. Lv H, *et al.* "Ionic Liquid Catalyzed C-C Bond Formation for the Synthesis of Polysubstituted Olefins". *European Journal of Organic Chemistry* 2022.45 (2022): e202201222.
31. Zhuang H, *et al.* "Bu₄NHSO₄-Catalyzed Direct N-Allylation of Pyrazole and its Derivatives with Allylic Alcohols in Water: A Metal-free, Recyclable and Sustainable System". *Advanced Synthesis and Catalysis* 363.24 (2021): 5461-5472.
32. Lu N, *et al.* "Theoretical investigation on transformation of Cr (II) to Cr (V) complexes bearing tetra-NHC and group transfer reactivity". *International Journal of Quantum Chemistry* 120 (2020): e26340.
33. Lu N, *et al.* "Theoretical investigation on the mechanism and enantioselectivity of organocatalytic asymmetric Povarov reactions of anilines and aldehydes". *International Journal of Quantum Chemistry* 120 (2020): e26574.
34. Frenking, G, *et al.* "The Nature of the Bonding in Transition-Metal Compounds". *Chemical Review* 100.2 (2000): 717-774.
35. Becke AD. "Density-functional thermochemistry. IV. A new dynamical correlation functional and implications for exact-exchange mixing". *The Journal of Chemical Physics* 104.3 (1996): 1040-1046.
36. Lee CT, *et al.* "Development of the Colle-Salvetti correlation-energy formula into a functional of the electron density". *Physical Review B* 37.2 (1988): 785-789.
37. Tapia O. "Solvent effect theories: Quantum and classical formalisms and their applications in chemistry and biochemistry". *Journal of Mathematical Chemistry* 10.1 (1992): 139-181.
38. Tomasi, J, *et al.* "Molecular Interactions in Solution: An Overview of Methods Based on Continuous Distributions of the Solvent". *Chemical Review* 94.7 (1994): 2027-2094.

39. Simkin BY, *et al.* "Quantum Chemical and Statistical Theory of Solutions—A Computational Approach". Ellis Horwood, London (1995).
40. Tomasi J, *et al.* "Quantum Mechanical Continuum Solvation Models". *Chemical Review* 105.8 (2005): 2999-3093.
41. Marenich AV, *et al.* "Universal solvation model based on solute electron density and on a continuum model of the solvent defined by the bulk dielectric constant and atomic surface tensions". *The Journal of Physical Chemistry. B* 113.18 (2009): 6378-6396.
42. Reed AE, *et al.* "Natural population analysis". *The Journal of Chemical Physics* 83.2 (1985): 735-746.
43. Reed AE, *et al.* "Intermolecular interactions from a natural bond orbital donor-acceptor view point". *Chemical Review* 88.6 (1988): 899-926.
44. Foresman, JB, *et al.* "Exploring Chemistry with Electronic Structure Methods". 2nd ed., Gaussian, Inc., Pittsburgh (1996).
45. Lu T, *et al.* "Multiwfn: A multifunctional wavefunction analyzer". *Journal of Computational Chemistry* 33.5 (2012): 580-592.